Effect of Particle Size on the Adsorption of O and S Atoms on Pt: A Density-Functional Theory Study

Xi Lin

Department of Chemistry, Massachusetts Institute of Technology, Cambridge, Massachusetts 02139-4301

Nicholas J. Ramer[†] and Andrew M. Rappe

Department of Chemistry and Laboratory for Research on the Structure of Matter, University of Pennsylvania, Philadelphia, Pennsylvania 19104-6323

Kenneth C. Hass and William F. Schneider

Department of Chemistry and Environmental Science, Ford Research Laboratory, MD 3083-SRL, Dearborn, Michigan 48121-2053

Bernhardt L. Trout*

Department of Chemical Engineering, Massachusetts Institute of Technology, Cambridge, Massachusetts 02139-4301

Received: March 27, 2001; In Final Form: May 30, 2001

In order to evaluate the effect of size on the adsorption energies on small Pt particles, we have performed a series of DFT-GGA calculations on Pt clusters of varying sizes, between 3 and 25 atoms, and a Pt(111) slab, with and without O and S adsorbates. We have found a significant variation in the energy of adsorption as a function of cluster size. In particular, energies of adsorption on the Pt_{10} cluster showed the largest deviation from those on the slab surface. Structural and energetic properties compare excellently to published experimental data. The Pt_4 clusters with and without adsorbates were found to have reduced symmetry due to the Jahn−Teller effect. A simple rule between the cohesive energy and the size of small close-packed platinum particles is derived and confirmed by our first-principle calculations, the extrapolation of which excellently matches both experimental and computational bulk cohesive energies.

I. Introduction

A goal in the field of catalysis is to be able to adjust the structure of catalytic materials to obtain the optimal electronic properties for desired chemical reactivity. The difficulty of achieving this goal is compounded by the fact that in many processes, a single component of a catalyst can be involved in many different reactions, some desired and others not. For example, Pt is a major component in current automobile three-way catalysts, in which it is used primarily to oxidize CO and residual hydrocarbons.[1] In addition, it is a proposed oxidizing component in a new class of automotive catalysts called lean-NO_x trapping catalysts. One of the obstacles to the use of lean-NO_x trapping catalysts is the lack of selectivity for NO over SO_2 oxidation by the Pt particles, leading to the generation of SO_3, and ultimately sulfation and poisoning of the NO_x traps. Thus, it would be desirable to optimize the structure of Pt catalyst particles to be selective against the oxidation of SO_2.

As a step toward understanding how the structure of catalyst particles affects these functions, we have studied the effect of the size of Pt clusters, including the infinite Pt(111) surface, on the energy of adsorption of O atoms and S atoms. To accomplish this, we have chosen to use density functional theory[2,3] with plane-wave basis functions. This approach allows us to study in a consistent way the binding energies of O and S atoms on both isolated clusters and on slab models of infinite surfaces. It allows us to study well-defined systems and to probe directly properties of interest.

Density functional theory has been used in the past to compute the energy of adsorption of O and S atoms on various Pt surfaces.[4−12] In each study, the energy of adsorption of O atoms has been computed on either the infinite Pt surface or on Pt clusters. To our knowledge, no computational study has been performed to investigate the effect of size on the energy of adsorption of species on Pt clusters and slab using a consistent methodology. On the other hand, the size dependence effect on chemisorption of various species has been studied on some other metal surfaces.[13−17] Unfortunately, no general rule has been extracted and clearly verified. In addition, many researchers used fairly small clusters as representative of an extended catalyst surface. In this work, we test the reliability of such an approach.

Our objectives are to (1) validate the particular methodology used vis-à-vis both computational and experimental results already in the literature, (2) determine the effect of cluster size on the energetics of adsorption of species using a consistent methodology, and (3) evaluate the differences in the energetics of O and S atoms on various Pt clusters.

* Author to whom all correspondence should be addressed. E-mail: trout@mit.edu.

[†] Present address: Department of Chemistry, Long Island University − C. W. Post Campus, Brookville, NY 11548.

10.1021/jp011133p CCC: $20.00
Published on Web 07/19/2001

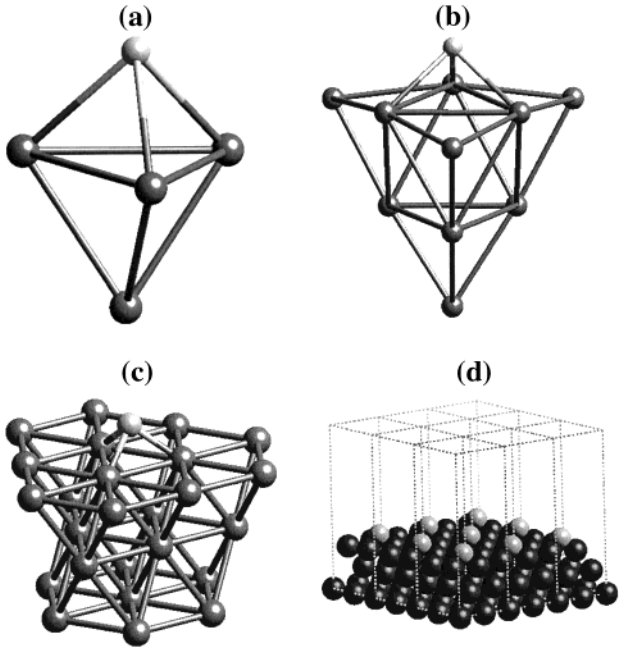

Figure 1. Computational models of the Pt(111) surface with adsorbed O/S atoms. (a) Pt_4−O/S. (b) Pt_{10}−O/S. (c) Pt_{25}−O/S. (d) Pt(111) slab with p-(2 × 2)−O/S.

II. Methodology

DFT Methods and Models. Kohn−Sham density functional theory was used for the cluster and slab calculations. The code used throughout was CPMD V3.3,[18] which uses plane-wave basis sets and employs periodic boundary conditions. In addition, an atomic pseudopotential generation code[19] was used to create highly transferable pseudopotentials (see below). For a couple of simple reference calculations, the Gaussian-94 package[20] was also used. In order to study isolated platinum clusters, supercells were used with no less than 10 Å of vacuum between periodic images. Three-layer slab models, consisting of 12 atoms were used to mimic infinite Pt(111) surfaces, and 10 Å of vacuum was included between the slabs. In both of these cases, the spacing was large enough such that results were insensitive to the size of the supercell used. Because of computational cost, thicker slabs were not tested in this study. Pictures of O/S adsorbed on clusters and on the slab are presented in Figure 1. All of these models were chosen because they contain 3-fold sites (fcc-like or hcp-like), the most active for atomic binding to their surface. During geometry optimization, all atoms are allowed to relax, except for those in the bottom layer of the slab model, which are fixed at the bulk distance.

Both PW91[21] and PBE[22] functionals were used, in addition to designed nonlocal pseudopotentials (see more details below). Scalar-relativistic pseudopotentials were used for Pt, and non-relativistic pseudopotentials were used for O and S. A plane-wave cutoff of 58 Ry was used for the calculations involving O and both 50 and 58 Ry were used for calculations involving S.

For the slab and bulk calculations, the free energy functional introduced by Alavi et al.[23] was used. This allows partial occupation[24] of electronic states via Fermi−Dirac statistics, and is related to the Mermin free energy functional.[25,26] An electronic temperature of 600 K was used for all of these calculations. The Trotter approximation was used with the Bogliubov correction[23] to evaluate the free energy functional. Lanczos diagonalization was used on the density matrix,[27] and convergence of the electronic density was achieved using Broyden mixing.[28] For cluster calculations, both the direct inversion in the iterative subspace (DIIS) method[29,30] of residual norm minimization and the preconditioned conjugated gradient (PCG)[31,32] or steepest descent (ST)[33,34] minimization in total energy minimization methods were used for wave function optimization. The DIIS method was also combined with the BFGS quasi-Newton method[35] to optimize ionic geometries in both slab and cluster calculations.

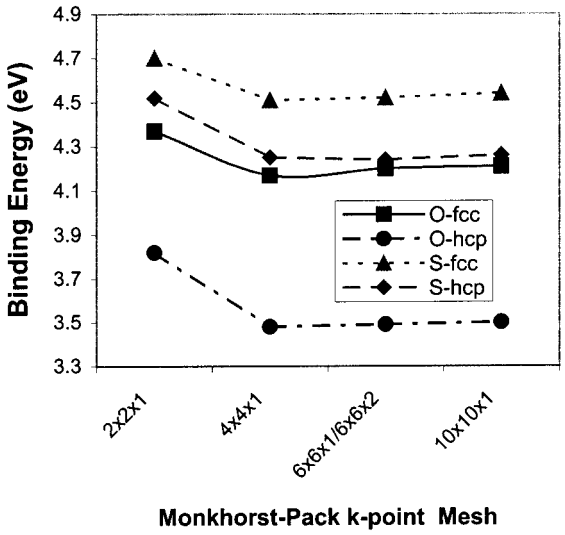

Figure 2. Convergence of *k*-point sampling. The 6 × 6 × 2 Monkhorst-Pack mesh is used for O-fcc and O-hcp. The 6 × 6 × 1 Pack-Pack mesh is used for S-fcc and S-hcp.

For the slab calculations, various numbers of *k*-points were tested using a Monkhorst-Pack mesh. The results are reported in Figure 2. Note that geometry optimization was performed for the 2 × 2 × 1 mesh and for the 4 × 4 × 1 mesh. Calculations performed with additional numbers of *k*-points used the optimized geometry for the 4 × 4 × 1 mesh. Sufficient convergence is achieved with the 4 × 4 × 1 mesh, consisting of 16 *k*-points (9 symmetry unique *k*-points).

Designed Nonlocal Pseudopotentials. To strive for maximum accuracy and transferability, we have chosen to use designed nonlocal (DNL) pseudopotentials,[36] which are norm-conserving,[37] nonlocal,[38] optimized[39] pseudopotentials. In these DNL pseudopotentials, one or two augmentation operators (usually step functions) are added to the local part of the pseudopotential and then are subtracted from the nonlocal part of the pseudopotential. By adjusting the augmentation operator, very precise agreement can be obtained between all-electron eigenvalues and pseudoeigenvalues for various atomic electronic configurations. During construction of the pseudopotentials, ghost states were detected and removed systematically.[40,41]

Relativistic effects were included in the pseudopotentials by solving the Dirac equation to obtain separate spin-up ($j = l + 1/2$) and spin-down ($j = l - 1/2$) pseudopotentials for each angular momentum channel (l). In practice, these two pseudopotentials are combined to create an average pseudopotential so that a Schrödinger-like equation can be used. This single pseudopotential is constructed by averaging over the two j-dependent relativistic pseudopotentials weighted by their degeneracies ($2j + 1$).[42,43] This procedure contains a minor error of order α^2, where α is the fine structure constant.

For each of the atoms, a reference configuration must be chosen, in addition to radial cutoffs and energy cutoffs for the projectors. For Pt, the chosen reference state configuration is $6s^1 6p^{0.1} 5d^{8.9}$, with radial cutoffs of 1.8, 2.4, and 1.6 Bohr and

TABLE 1: Transferability Test of Designed Non-local Pseudopotential for Atomic Sulfur[a]

configuration	all-electron energy	OPT energy error	DNL energy error
$3s^2$	−1.5393	0.0000	0.0000
$3p^{3.5}$	−0.7748	0.0000	0.0000
$3d^{0.5}$	−0.0318	0.0000	0.0000
$3s^{1.5}$	−1.7621	0.0015	0.0004
$3p^3$	−0.9688	0.0012	0.0004
$3d^{1.5}$	−0.0533	0.0000	0.0000
$3s^1$	−1.9103	0.0044	0.0015
$3p^2$	−1.0955	0.0039	0.0018
$3d^3$	−0.0911	−0.0001	−0.0003
$3s^2$	−2.0218	0.0003	−0.0002
$3p^3$	−1.2356	0.0002	−0.0002
$3d^0$	−0.2953	−0.0001	−0.0001
$3s^2$	−2.2092	0.0018	−0.0000
$3p^2$	−1.4044	0.0016	0.0001
$3d^1$	−0.4022	−0.0003	−0.0006
$3s^2$	−2.5201	0.0016	−0.0004
$3p^2$	−1.7055	0.0014	−0.0002
$3d^{0.5}$	−0.6590	−0.0004	−0.0006
$3s^2$	−1.5955	0.0001	−0.0000
$3p^{3.25}$	−0.8221	0.0001	−0.0000
$3d^1$	−0.0157	0.0000	0.0000

[a] All energy units are in Ry. Configuration $3s^2 3p^{3.5} 3d^{0.5}$ is the reference.

energy cutoffs of 37, 25, and 50 Ry for the 6s, 6p, and 5d pseudopotential projectors, respectively. A shorter radial cutoff of 1.2 Bohr for both s and p pseudopotential channels and higher energy cutoffs of 50 and 58 Ry for 2s and 2p, respectively, have been employed for O, because oxygen tends to form shorter bonds (e. g., the bond length of O_2 is 2.29 Bohr). For the S atom, it is crucial to include a 3d projector, not only for cases when sulfur binds to transition metals, but also for simple molecules, such as S_2 and SO. This 3d projector dramatically improves the quality of the norm-conserving pseudopotential. The reference configuration for S is $3s^2 3p^{3.5} 3d^{0.5}$, with radial cutoffs of 1.3, 1.3, and 2.2 Bohr and an energy cutoff of 50 Ry for all s, p, and d projectors.

Each of the pseudopotentials used in this study has a maximum transferability error of a few mRy (1 mRy = 1.3 kJ/mol). This error is determined by comparing the eigenvalues of nonreference configurations determined using the generated pseudopotential with those generated via an all-electron calculation. Examples of these errors for the S pseudopotential are found in Table 1. The optimized pseudopotential (OPT) energy error is for the pseudopotential without the augmentation operator and the designed nonlocal pseudopotential (DNL) energy error is for the pseudopotential with the augmentation operator, which is the one used in this study.

III. Results and Discussion

A. Diatomics. In Table 2, results for representative diatomic gas-phase molecules are presented, with comparisons to all-electron calculations and to experimental results. All Kohn−Sham spin−orbitals had an occupancy set to either 1 or 0. Table 3 shows several spin-excited energies of Pt_2, PtO, and PtS with respect to their corresponding electronic ground states, all of which have a spin of 1. Discrepancies between the bond energies of O_2 and SO calculated using the designed nonlocal pseudopotential method and calculated by treating all of the electrons explicitly are ∼20−30 kJ/mol. Since there is almost no discrepancy for the case of S_2, we attribute the differences to the difficulty in treating the 2p states of oxygen and the need for a very small radial cutoff for oxygen pseudopotentials.[44] Almost all of the calculated bond energies are greater than the experimental ones, as is typical in density functional theory.

TABLE 2: Molecular Transferability Test of Designed Non-local Pseudopotential (All calculations are performed with DFT-PBE spin-polarized functionals. All molecules in the table have a spin of 1. The number in parentheses shows the experimental uncertainty.)

bond energy (kJ/mol)	DNL	all-electron	experiment	other calculations
O_2	606.0	579.1[a] 569.9[b]	493.6[c]	
S_2	481.9	480.2[a] 465.7[b]	421.6[c]	
Pt_2	278.0		303(2)[d] 354.8(4.6)[e] 357.9(59.0)[e] 288, 292, 253[f]	220, 190[g] 111−147[h] 318[i] 349.9[j]
SO	583.2	558.3[a] 569.0[b]	517.1	
PtO	455.4		366.6[c]	
PtS	416.4			

bond length (Å)	DNL	all-electron	experiment	other calculations
O_2	1.20	1.22[a]	1.21[c]	
S_2	1.91	1.92[a]	1.89[c]	
Pt_2	2.29		2.34[e]	2.40, 2.46[g] 2.65(1)[h] 2.40[i] 2.36[j]
SO	1.50	1.52[a]	1.48[c]	
PtO	1.69		1.73[c]	
PtS	2.03			

[a] Gaussian94 (UBPW91/cc-PVTZ). [b] DFT LSDA plus Becke exchange correction plus PW91 correlation correction.[45] [c] Ref 46. [d] Resonant two-photon ionization spectroscopy.[47] [e] Kundsen cell mass spectrometry and empirically estimated bond length.[48] [f] Empirical atomic cell model.[49−51] [g] CASSCF−FOCI, without and with spin−orbital interactions.[52] [h] HF and post-HF.[53] [i] DFT-LDA (Harris functional[54]).[55] [j] DFT-GGA.[56]

The computed Pt_2 binding energy of 278.0 kJ/mol is at the lower end of the wide range of experimental results, 253−357.9 kJ/mol. Recent theoretical works showed an even larger spread, from 111 to 350 kJ/mol. Because of the importance of relativistic effects, which are very expensive to include in all-electron calculations, we are unable to compare our pseudopotential results with related all-electron results. In addition, the large variation in reported experimental Pt_2 binding energies also precludes an accurate comparison. Accurate comparison, however, will be possible with bulk platinum (see below).

B. Bonding of Pt Clusters, Slabs, and Bulk Metal. Since one of the major objectives of this work is to investigate the effect of cluster size on the energy of adsorption of adatoms, small clusters were chosen that contain sites similar to the most active sites on a Pt(111) surface. These are 3-fold (both fcc-like and hcp-like) sites. In particular, clusters containing 3, 4, 10, and 25 Pt atoms were studied; examples are shown in Figure 1a−c. The 3-fold site in Pt_4 is similar to an hcp site, and the 3-fold sites in the middle of the Pt_3, Pt_{10}, and Pt_{25} clusters are similar to fcc sites.

Structural data for the relaxed clusters are presented in Figure 3. Pt_3 adopts an equilateral triangle (D_{3h} symmetry) with a triplet ground state. The edge distance of 2.45 Å is significantly less than that found in bulk Pt and somewhat less than the 2.52 Å found in a recent DFT study of by Kua and Goddard.[56] We

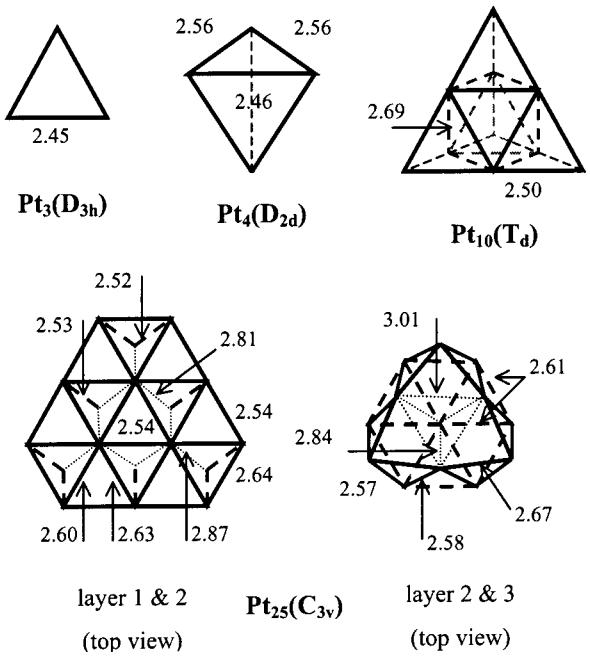

Figure 3. Optimized geometry of Pt clusters. Note that the Pt_{25} clusters are separated into two diagrams for clarity, the diagram on the left being the first two layers and the diagram on the right being the second and third layers. Both solid and dashed lines represent normal chemical bonds between species, while dots are for those bonds longer than 2.77 Å (bulk bond length).

TABLE 3: Determination of the Optimal Spin States with the Spin-Polarized PBE Functional

	spin	excited-state energy (kJ/mol)	bond length (Å)
PtO	3	678.2	1.87
	2	146.5	1.79
	0	125.4	1.71
	1	0	1.69
PtS	3	657.3	2.28
	2	171.4	2.18
	0	97.29	2.03
	1	0	2.03
Pt_2	3	443.8	2.40
	0	69.8	2.28
	2	55.5	2.26
	1	0	2.29
Pt_3	0	23.9	
	2	19.9	
	1	0	
Pt_3O	0	64.9	
	1	23.0	
	2	0	
Pt_3S	0	0.6	
	2	0	
Pt_4	0	111.6	
	3	56.37	
	1	19.3	
	2	0	
Pt_4O	0	69.21	
	1	0	
Pt_4S	3	78.2	
	0	41.9	
	2	22.5	
	1	0	
Pt_{10}	0	139.3	
	4	0	

find a singlet−triplet splitting of 23.9 kJ/mol, about 10 kJ/mol larger than that found previously.[56]

Several recent studies have reported Pt_4 to have a tetrahedral structure. We find Pt_4 to have a distorted tetrahedral (D_{2d} symmetry) relaxed geometry and a quintet ground state. This symmetry lowering can be attributed to the Jahn−Teller[57] effect. According to the Jahn−Teller theorem, the total energy of a nonlinear molecular with a degenerate ground state can always be lowered by reducing the symmetry of the nuclear configuration. The T_d-constrained Pt_4 cluster has a singly occupied, triply degenerate HOMO level (explicitly $(e)^2(a)^1(t)^1$ in the majority spin) and is 31 kJ/mol higher than that of the relaxed D_{2d} structure.

The symmetry lowering that we observed was not reported for Pt_4 in a couple of recent calculations, ab initio CAS-MCSSCF (by Dai and Balasubramanian[58]) and DFT-GGA (by Kua and Goddard[56]), although Yang et al.[55] were not able to find a stable tetrahedral structure for Pt_4 in their spin-paired, nonself-consistent Harris functional LDA study. We note that their spin-paired calculations of a larger cluster, Pt_{13}, resulted in only a 0.3 kJ/mol lower energy for a distorted structure versus a symmetric one. When spin is considered explicitly for the Pt_{13} cluster, the energy of a distorted structure becomes 8 kJ/mol lower than that of the symmetric one, as reported in a DFT-GGA study by Watari et al.[59] We also note that Kua and Goddard[56] reported a ground-state spin of 1 for Pt_4, using GGA. An abundance of other metal clusters are reported to contain significant distortion, attributed to the Jahn−Teller effect, including Ni_3−Ni_{10} (tight-binding MD),[61] Nb_n (n = 3−7) (DFT),[62] Pd_{13} (DFT),[55,59] Au_3 (CCSD),[63] Au_{13} (Dirac scattered-wave),[64] as are nontransition metals and semiconductors, such as Li_n (n = 4, 6, 8, 14, and 16) (UHF),[65] Li_7 (molecular beam electron spin resonance),[66] Al_n (n = 13, 19, 23, and 55) (DFT),[67,68] Si_n (n = 3−14) (tight-binding and DFT),[69] and Sn_3^- (anion photoelectron spectrum).[70] In summary, all of our calculations indicate that the Jahn−Teller effect leads to a distorted structure for Pt_4, and this finding is in agreement with available results on small clusters of other metals.

Atoms in the Pt_{10} cluster are connected by bonds of different length, 2.50 Å between a corner atom and an edge atom, and 2.69 Å between two edge atoms. The Pt_{10} cluster maintains T_d symmetry. It possesses a doubly degenerate HOMO level, but in this case, as opposed to the Pt_4 cluster, the HOMO level is fully occupied, leading to no Jahn−Teller effect. In general, the bonds in this Pt_{10} cluster are longer than the bonds in Pt_4.

The relaxed Pt_{25} cluster is only slightly distorted from C_{3v} symmetry, as shown in Figure 3. More importantly, bonds in the middle layer are significantly longer than bonds in the bulk Pt (2.77 Å). This is due to the much lower coordination of atoms in the middle layer versus geometrically equivalent atoms in the extended Pt(111) surface. This low coordination has several significant consequences. First, the bonds in the middle layer are as long as 3.01 Å. Second, the bonds between the second-layer edge atoms and the central atoms of the top and bottom layers also get stretched to 2.81 and 2.84 Å long, respectively. Third, the bonds between these second-layer edge atoms and the edge atoms of the top layer become the shortest in the cluster (2.51−2.52 Å). The bonds between the atoms on the bottom layer are quite uniform and have an intermediate bond length value of 2.61 Å, which is still quite different from the bulk value.

For bulk (fcc) Pt, we have computed a lattice constant of 3.921 Å and a cohesive energy of 562.8 kJ/mol. Both of these agree excellently with the experimental values of 3.92 Å and 564.4 kJ/mol.[71]

The Pt(111) slab surface does not experience in-plane reconstruction, and has only a 2% contraction in the interlayer spacing. This can be compared with the experimental value of

TABLE 4: Destabilization Energy of Cluster[a]

	number of atoms	cohesive energy (kJ/mol)	destabilization energy (kJ/mol)
Pt_2	2	138.9	424.5
Pt_3	3	192.0	373.4
Pt_4	4	233.5	330.0
Pt_{10}	10	336.7	226.8
Pt_{25}	25	369.5	193.9
Pt bulk (exp.)		563.5	0

[a] The destabilization energy is defined as the cohesive energy in the bulk minus the cohesive energy in the cluster.

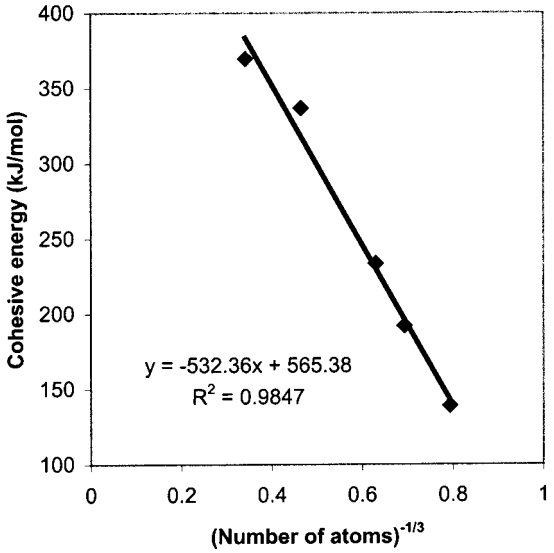

Figure 4. Cohesive energy versus the number of atoms to the −1/3 power.

a slight increase of 1%.[71] Thus, the local geometry of the adsorption sites on the Pt(111) slab is significantly different than those in the cluster models chosen in this study. The difference can be further enhanced during the surface reconstruction caused by the chemisorption of atoms, an effect that will be discussed in detail in section D.

C. Cohesive Energy of Small Clusters. The destabilization energy of a cluster, defined as the cohesive energy of the bulk minus the binding energy per atom in the cluster, will be proportional to the surface area of the cluster for large clusters. The surface area of the cluster is in turn proportional to the number of atoms to the power of 2/3. Therefore, the destabilization energy per atom in a cluster should be proportional to the number of atoms to the power of −1/3.

$$E_d(n) = E_c(bulk) - E_c(n) \propto \frac{1}{n}(r^2) \propto \frac{1}{n}(n^{2/3}) = n^{-1/3}$$

This simple argument for large clusters is born out by our ab initio DFT calculations on small Pt clusters. The data are collected in Table 4 and plotted in Figure 4. When the cohesive energy is assumed to increase with the number of atoms to the power of −1/3, an excellent linear fit results. By extrapolating the cohesive energy to the cluster with an infinite size, an energy of 565.4 kJ/mol is obtained. This extrapolated bulk cohesive energy value excellently matches the experimental and computational results for Pt bulk (562.8 and 564.4 kJ/mol, respectively).

This apparently straightforward rule is rather surprising since the clusters studied in this paper contain only 25 atoms or fewer. Although the implied close-packed structure should be considered as a favored factor for the rule, it is not obvious that a Pt dimer or trimer can be viewed as a spherical particle. Of course, we expect an even better agreement for larger and rounder Pt clusters.

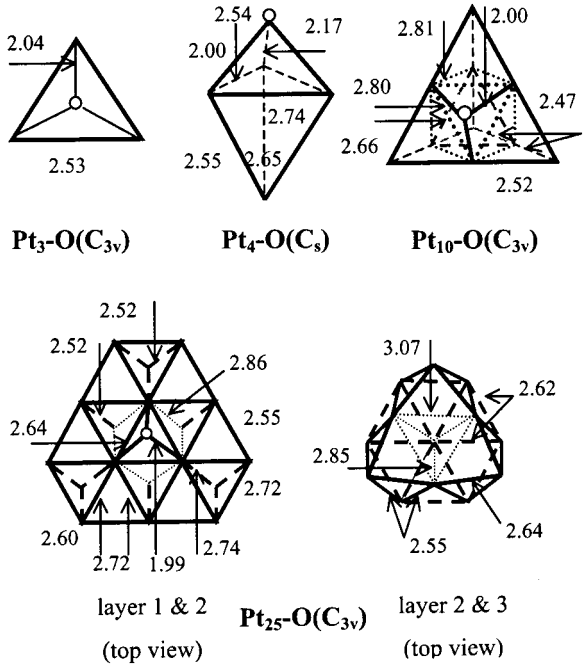

Figure 5. Optimized geometry of Pt clusters with O adsorbates. Note that the Pt_{25} clusters are separated into two diagrams for clarity, the diagram on the left being the first two layers and the diagram on the right being the second and third layers. Both solid and dashed lines represent normal chemical bonds between species, while dots are for those bonds longer than 2.77 Å (bulk bond length). Circles represent O atoms.

Recently, a rather different rule was proposed by Kua and Goddard[56] from their DFT-GGA study on small Pt clusters. They claimed that a constant amount of cohesive energy should be added to the clusters for clusters sizes from $n = 2$ to 10. Such a conclusion was a result of their choosing a nonstandard definition of cohesive energy, and when the standard definition is used, their data follow the same rule as ours.

D. Adsorption on Surfaces. Energies of adsorption of O and the S atoms on the clusters and the slabs are presented in Table 5 and compared with experimental data and other calculations. Structural properties of the clusters with adsorbates are found in Figures 5 and 6. In addition, Table 6 shows the bond length between adsorbates and Pt atoms. For all the clusters that have more than one single layer, there is only a slight variation with cluster size and generally good agreement with experiment. By contrast, there is no simple trend for the binding energy with respect to the size of the cluster. Moreover, there is no simple trend for the binding energy with respect to the HOMO energy levels of the clusters, as shown in Table 5.

The Pt_3 cluster possesses a perfect C_{3v} symmetry after the adsorption of atomic oxygen or sulfur. The distance between the O and S adsorbates and the Pt atoms is 0.03 and 0.04 Å greater than the analogous distances on the fcc slab, and the adsorbate binding energies are 30 and 7 kJ/mol less than the binding energies in the slab calculations, respectively. These differences in energy are rather small given the small size of the cluster, and suggest that the Pt_3 cluster could provide a fairly good approximation to a Pt(111) fcc site for energetic studies.

Upon adsorption of oxygen or sulfur, the symmetry of the Pt_4 cluster is reduced from D_{2d} to C_s. Although the adatom is still at a 3-fold site, it is closer to two Pt atoms and farther

TABLE 5: Energy of Chemisorptions of Atomic Oxygen and Sulfur on Pt Clusters and Slab (In the cases for the cluster models where there are two values separated by a slash, the first entry is with the PBE functional and the second entry is with the PW91 Functional. The LUMO levels of O and S are −6.20 and −5.58, respectively.)

model (spin without adsorbates)	HOMO energy (eV)	binding energy of oxygen in kJ/mol (spin with adsorbate)	binding energy of sulfur in kJ/mol (spin with adsorbate)
Pt-1 (triplet)	−6.09	455.4 (triplet)	416.4 (triplet)
Pt-3 (triplet)	−4.82	376.6 (quintet)	431.1 (quintet)
Pt-4 (quintet)	−4.59	317.7/317.3 (triplet)	447.7/439.8 (triplet)
Pt-10 (nonet)	−4.70	191.6/195.7 (singlet)	338.6/336.2 (singlet)
Pt-25 (singlet)	−5.15	368.6 (singlet)	434.4 (singlet)
Pt(111) fcc		406.5	438.5
Pt(111) hcp		337.7	410.8
experiments at fcc sites		417(32), 405(34)[a]	375[k]
		353, 347, 353, 347[b]	
other calculations at fcc sites		290[c]	183[l]
		509[d]	95, 480, 386, 394, 135[m]
		500, 398[e]	
		251, 276[f]	
		−244, 261, 206, 252, −142[g]	
		−143, −73[h]	
		492[i]	
		427[j]	

[a] Single-crystal adsorption calorimetry.[72, 73] [b] Temperature-programmed desorption.[74−77] [c] MO−atom superposition and electron delocalization; planar Pt_4 cluster.[4] [d] LCAO-LDA; mid-terrace of stepped surfaces.[5] [e] DFT-LDA and post-GGA; 6-layer slab.[6] [f] MO-GGA, double-ζ and triple-ζ STO basis sets; Pt_{10} cluster.[7] [g] HF, SRMP2, MRMP2, MRCI, and DFT-VWN (LSD); Pt_9 cluster.[8] [h] HF and DFT-VWN (LSD); Pt_{25} cluster.[8] [i] DFT-GGA FP-LAPW; 5-layer slab.[9] [j] DFT-post-GGA, 4-layer slab.[10] [k] Temperature-programmed desorption.[78] [l] HF double-ζ basis set; Pt_{12} cluster.[11] [m] HF, SRMP2, MRMP2, MRCI, and DFT-VWN (SIC); Pt_{25} cluster.[12]

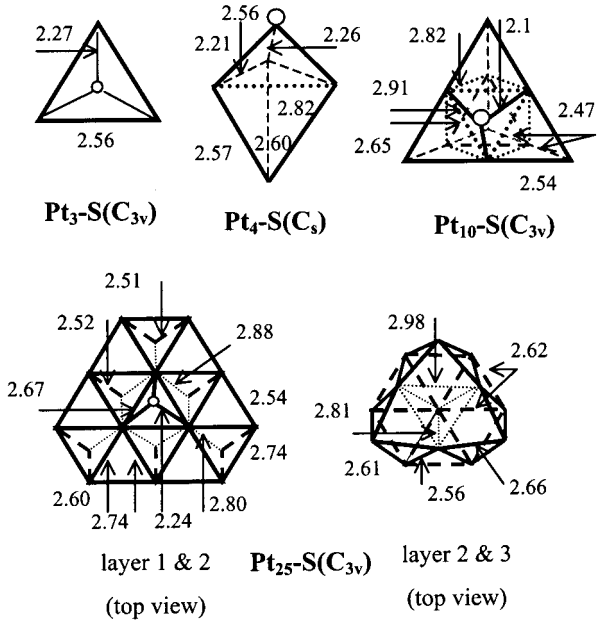

Figure 6. Optimized geometry of Pt clusters with S adsorbates. Note that the Pt_{25} clusters are separated into two diagrams for clarity, the diagram on the left being the first two layers and the diagram on the right being the second and third layers. Both solid and dashed lines represent normal chemical bonds between species, while dots are for those bonds longer than 2.77 Å (bulk bond length). Circles represent S atoms.

away from the third. Adsorption results in an increase in all the Pt−Pt distances. Pt−O and Pt−S bond distances are closer to those found for O and S adsorption on an hcp site of Pt(111). The O binding energy decreases by about 60 kJ/mol from Pt_3 to Pt_4, comparable to the difference between fcc and hcp sites on the Pt(111) slab. In contrast, the S binding energy increases by approximately 10 kJ/mol from Pt_3 to Pt_4, compared to a 20 kJ/mol decrease from the fcc to hcp site on Pt(111). Thus, while Pt_3 and Pt_4 approximate the local adsorption at fcc and hcp sites well, the small size leads to distinct energetic differences with adsorption on the Pt(111) surface.

TABLE 6: Bond Length (in Å) between the Adsorbate and the nearest Pt Atoms

model (spin without adsorbates)	O−Pt bond length (spin with adsorbate)	S−Pt bond length (spin with adsorbate)
Pt-1 (triplet)	1.69 (triplet)	2.03 (triplet)
Pt-3 (triplet)	2.04 (quintet)	2.27 (quintet)
Pt-4 (quintet)	2.00 (triplet)	2.21 (triplet)
Pt-10 (nonet)	2.00 (singlet)	2.19 (singlet)
Pt-25 (singlet)	1.99 (singlet)	2.24 (singlet)
Pt(111) fcc	1.99	2.25
Pt(111) hcp	2.00	2.24
experiments at fcc sites	1.99(3)[a]	2.28(3)[b]
other calculations at fcc sites	1.61[c]	2.33[i]
	2.00[d]	2.41−2.47[j]
	1.99[e]	
	2.09, 2.03[f]	
	2.07−2.21[g]	
	2.02[h]	

[a] Low-energy electron diffraction.[79] [b] Low-energy electron diffraction.[80] [c] MO − atom superposition and electron delocalization; planar Pt_4 cluster.[4] [d] LCAO-LDA; mid-terrace of stepped surfaces.[5] [e] DFT-LDA and post-GGA; 6-layer slab.[6] [f] MO-LDA, double-ζ and triple-ζ STO basis set; Pt_{10} cluster.[7] [g] HF, SRMP2, MRMP2, MRCI, and DFT-VWN (LSD); Pt_9 and Pt_{25} clusters.[8] [h] DFT-post-GGA, 4-layer slab.[10] [i] HF double-ζ basis set; Pt_{12} cluster.[11] [j] HF, SRMP2, MRMP2, MRCI, and DFT-VWN (SIC); Pt_{25} cluster.[12]

For the Pt_{10} cluster, adsorption on one of the four (identical) surfaces lowers the original T_d symmetry to C_{3v} symmetry. In addition, upon adsorption, all of the bonds between the atoms in the top layer and the middle layer become stretched. Moreover, the binding energy of both oxygen and sulfur atoms is the lowest of all of the models in this study, 191.62 and 338.59 kJ/mol, respectively, indicating that the electronic structure of this cluster is much different from that of the slab. These results suggest that this 10-atom Pt cluster is a poor model of the Pt(111) surface, particularly for the adsorption of atoms.[7]

This issue associated with the adsorption on the Pt_{10} cluster raises the importance of performing further studies on a much larger cluster, such as the Pt_{25} cluster, to examine the particle-size effect on the adsorption reactivity of clusters compared to

TABLE 7: Relaxation of the Pt(111) Slab upon Adsorption of Atomic Oxygen and Sulfur[a] .

Å	d_{01}	d_{12}	d_{23}	b_1	B_2
O-fcc	1.14	2.25	2.23	0.16	−0.11
exp.[b]	1.18(2)	2.29(3)	2.26(5)	0.07(3)	−0.09(10)
O-hcp	1.24	2.26	2.24	0.29	−0.02
S-fcc	1.56	2.26	2.24	0.18	−0.09
S-hcp	1.61	2.26	2.24	0.29	−0.04

[a] No symmetry constraints are enforced for the relaxation. Negative value indicates a deviation toward the adatom. Refer to Figure 7 for definitions of quantities in this table [b] Low-energy electron diffraction.[79]

the slab. The Pt_{25} cluster that we chose contains all of the three Pt atoms of an fcc site, a complete set of their first neighbors, and several of their second and third neighbors. As shown in Table 5, however, there still exists a significant difference between this fairly large cluster and the infinite slab for both atomic oxygen and sulfur chemisorption. On the other hand, because of the inclusion of a complete set of the first neighbors on the top layer, the local structure of the substrate is similar to that of the slab for both the fcc and hcp sites. In addition, as shown in Table 6, the distance between the S atom and the Pt atoms is the same for the Pt_{25} cluster and the slab. Therefore, while as few as four Pt atoms are sufficient to generate a Pt−O bond with the same length as that on the slab, a three-layer model with a complete set of first-neighbors is necessary for a Pt−S bond to have the same length as that on the slab. Finally, as in the case of Pt_{10}, the stretched bonds of the second-layer atoms decrease the capability of the Pt_{25} cluster to stabilize the adsorbates.

A conclusion from Table 5 is that there is a wide variation in the energies of adsorption of both O and S atoms on the various clusters and the slab. For all cases, except for the Pt atom, the energy of adsorption of S is greater than that of O. This can be explained by the S atom having relatively low-lying unoccupied 3d orbitals, which can receive electrons from the Pt and can mix with the 5d electrons of the Pt.

However, there is no trend that can be discerned for the energies of adsorption as a function of cluster size, and for the case of the O atom, the energy of adsorption on the 25 atom Pt cluster is still much different from that on the slab. Thus, clusters as large as 25 Pt atoms still differ significantly in their chemistry from the bulk Pt surface. That Pt_3 behaves similarly in O and S adsorption to an fcc site on Pt(111) is apparently accidental, because in larger fcc cluster models, the agreement becomes poorer, and in the Pt_{10} case the differences are remarkably large.

Our calculated energy of adsorption of O at the fcc site, 407 kJ/mol, is within 0−10 kJ/mol of the two experimental values determined via microcalorimetry on the Pt(111) surface with 0.25 monolayer coverage.[72,73] Because of the nature of the experiment, we believe that these are much more accurate than the values extrapolated from TPD data.[74−77] Most other calculations have substantially greater error, except for the DFT post-GGA studies (GGA energy evaluations using the LDA densities) by Bogicevic et al.[6] and Bleakley and Hu.[10] With a model of 6-layer slab for the Pt(111) surface, Bogicevic et al. obtained a binding energy of 398 kJ/mol, about 9 kJ/mol lower than from our 3-layer slab model. Bleakley and Hu used a 4-layer slab (with the bottom 3 layers fixed at bulk geometry) and obtained a binding energy of 427 kJ/mol, which is 20 kJ/mol higher than ours.

Table 7 shows the local restructuring of the Pt atoms near the site of the adsorbates, and compares the calculated results with those measured on a system with a 0.25 monolayer coverage (p-(2 × 2)) by LEED.[79] Figure 7 shows this restructuring schematically. The errors with respect to experiment are generally a few hundredths of an Å. The error associated with the finite size of the supercell was explored by Jennison et al.[81] From their DFT-LDA study, at a distance of 5.5 Å, the lateral pair interaction energy of 7 kJ/mol for NH_3 and 2 kJ/mol for CO are obtained on a Pt_{91} cluster. Therefore, we believe that the lateral pair interactions in our study are also a few kJ/mol.

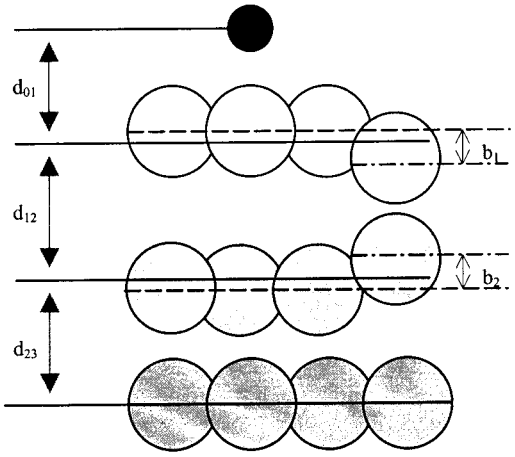

Figure 7. Schematic of the relaxation of the Pt slab with adsorbed O or S atoms. Refer to Table 7 for values. Note that 3-fold (both fcc and hcp) sites consist of the three Pt atoms to the left.

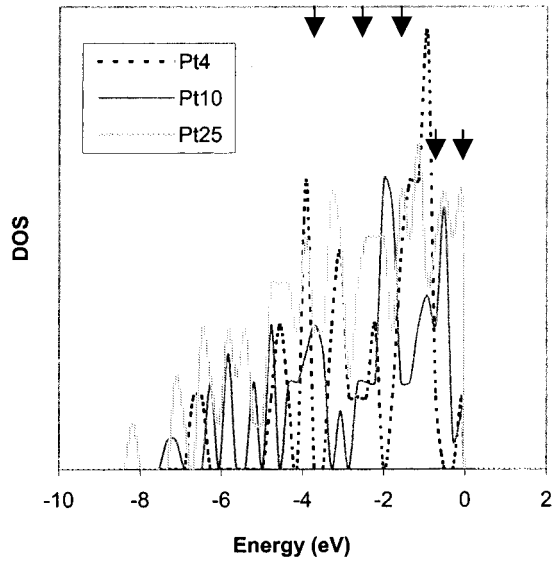

Figure 8. Density of states for the clusters. The zero of energy is taken as the HOMO level. Each curve is normalized to unit area. The arrows mark the five energy levels of atomic Pt.

The densities of states (DOS) of the cluster models are presented in Figure 8, which are aligned by their HOMO levels for a clear comparison. The absolute energies of the HOMO levels are collected in Table 5. As expected, for larger clusters, the energy range of DOS is larger, and the DOS profile is smoother. A comparison of the density of states of the 25-atom cluster to that of the slab is presented in Figure 9, where the HOMO level of the 25-atom cluster is aligned with the Fermi level of the slab. Simple reactivity rules do not emerge clearly from comparing these DOS.

IV. Conclusions

We have performed a series of DFT-GGA calculations on Pt clusters and a Pt(111) slab with and without O and S adsorbates. The Pt_4 cluster was significantly distorted from perfect sym-

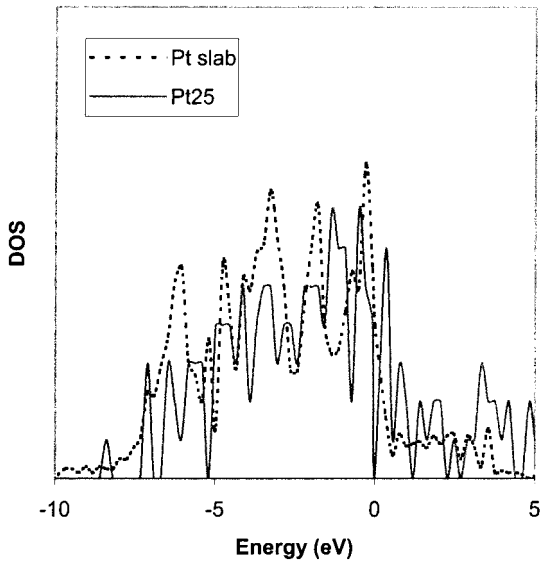

Figure 9. Comparison of the density of states between the 25-atom cluster and the slab model. The zero of energy for the 25-atom cluster is the HOMO level, and the zero of energy for the slab is the Fermi level.

metry, the Pt_3 and Pt_{10} cluster was not distorted, and the Pt_{25} cluster was only slightly distorted. These results can be excellently explained by the Jahn−Teller effect. In addition, the difference in the binding energy per atom between bulk Pt and small Pt clusters was proportional to the cluster size to the −1/3 power.

Adsorption of O on even up to a 25-atom cluster showed significantly different properties than that on the semi-infinite slab. Of all of the clusters studied, both larger and smaller, the 10-atom cluster was the most different from the slab, indicating that it is a poor model of the Pt(111) surface. By examining the size effects on the binding of atomic oxygen and sulfur to these 3-fold cluster models, one concludes that the reasonable agreement of energies of adsorption on small Pt clusters with those on extended systems is fortuitous, rather than systematic. These results also indicate that small clusters may exhibit significant differences in reactivity among themselves and between themselves and large particles. In all cases, except for the single Pt atom, the energy of adsorption of O on the semi-infinite slab was larger than that on each cluster, and the energies of adsorption of S were greater than those of O. In future work, we will explore the possible differences in reactivity for reactions with significance to lean-NO_x automotive catalysis.

Acknowledgment. We would like to thank Luke N. Shulenburger for the initial setup work of the 10-atom cluster calculations and Eric J. Walter and Ilya Grinberg for help in generation the pseudopotentials. Significant computational time was provided by the National Center for Supercomputing Applications. This work was supported by Ford Motor Company, NSF Grant under contract number CTS-9984301 and by the Office of Naval Research under contract number N-00014-00-1-0372.

References and Notes

(1) Taylor, K. C. *Catalysis − Science and Technology*; Anderson, J. R., Boudart, M., Eds.; Springer-Verlag: Berlin, 1984; *5*, 119.
(2) Hohenberg, P.; Kohn, W. *Phys. Rev.* **1964**, *136*, B864.
(3) Kohn, W.; Sham, L. J. *Phys. Rev.* **1965**, *140*, A1133.
(4) Ray, N. K.; Anderson, A. B. *Surf. Sci.* **1982**, *119*, 35.
(5) Feibelman, P. J.; Esch, S.; Michely, T. *Phys. Rev. Lett.* **1996**, *77*, 2257.
(6) Bogicevic, A.; Strömquist J.; Lundqvist, B. I. *Phys. Rev. B* **1998**, *57*, R4289.
(7) Chen, M.; Bates, S. P.; van Santen, R. A.; Friend, C. M. *J. Phys. Chem. B* **1997**, *101*, 10051.
(8) Illas, F.; Rubio, J.; Ricart, J. M.; Pacchioni, G. *J. Chem. Phys.* **1996**, *105*, 7192.
(9) Wilke, S.; Natoli, V.; Cohen, M. H. *J. Chem. Phys.* **2000**, *112*, 9986.
(10) Bleakley, K.; Hu, P. *J. Am. Chem. Soc.* **1999**, *121*, 7644.
(11) Rodriguez, J. A.; Chaturvedi, S.; Jirsak, T.; Hrbek, J. *J. Chem. Phys.* **1998**, *109*, 4052.
(12) Illas, F.; Clotet, A.; Ricart, J. M. *Catal. Today* **1999**, *50*, 613.
(13) Siegbahn, P. E. M.; Pettersson, L. G. M.; Wahlgren, U. *J. Chem. Phys.* **1991**, *94*, 4024.
(14) te Velde, G.; Baerends, E. J. *Chem. Phys.* **1993**, *177*, 399.
(15) Penev, E.; Kratzer, P.; Scheffler, M. *J. Chem. Phys.* **1999**, *110*, 3986.
(16) Wright, K.; Hillier I. H.; Vincent, M. A.; Kresse, G. *J. Chem. Phys.* **1999**, *111*, 6942.
(17) Dharma-wardana, M. W. C.; Zgierski, M. Z.; Ritchie, D.; Ping, J. G.; Ruda, H. *Phys. Rev. B* **1999**, *59*, 15766.
(18) Hutter, J.; Alavi, A.; Deutsch, T.; Bernasconi, M.; Goedecker, S.; Marx, D.; Tuckerman, M.; Parrinello, M. *CPMD*, version 3.3a; MPI für Festkörperforschung and IBM Zurich Research Laboratory: 1995−1999.
(19) A java version of the code is being developed. Refer to http://lorax.chem.upenn.edu./Education/QM/QMjava.html for more details.
(20) Frisch, M. J.; Trucks, G. W.; Schlegel, H. B.; Gill, P. M. W.; Johnson, B. G.; Robb, M. A.; Cheeseman, J. R.; Keith, T.; Petersson, G. A.; Montgomery, J. A.; Raghavachari, K.; Al-Laham, M. A.; Zakrzewski, V. G.; Ortiz, J. V.; Foresman, J. B.; Cioslowski, J.; Stefanov, B. B.; Nanayakkara, A.; Challacombe, M.; Peng, C. Y.; Ayala, P. Y.; Chen, W.; Wong, M. W.; Andres, J. L.; Replogle, E. S.; Gomperts, R.; Martin, R. L.; Fox, D. J.; Binkley, J. S.; Defrees, D. J.; Baker, J.; Stewart, J. P.; Head-Gordon, M.; Gonzalez, C.; Pople, J. A. *Gaussian 94*, revision E.3; Gaussian, Inc.: Pittsburgh, PA, 1995.
(21) Perdew, J. P.; Chevary, J. A.; Vosko, S. H.; Jackson, K. A.; Pederson, M. R.; Singh, D. J.; Fiolhais, C. *Phys. Rev. B* **1992**, *46*, 6671.
(22) Perdew, J. P.; Burke, K.; Ernzerhof, M. *Phys. Rev. Lett.* **1996**, *77*, 3865.
(23) Alavi, A.; Kohanoff, J.; Parrinello, M.; Frenkel, D. *Phys. Rev. Lett.* **1994**, *73*, 2599.
(24) Fernando, G. W.; Qian, G.; Weinert, M.; Davenport, J. W. *Phys. Rev. B* **1989**, *40*, 7985.
(25) Mermin, N. D. *Phys. Rev.* **1965**, *137*, A1441.
(26) Wentzcovitch, R. M.; Martins, J. L.; Allen, P. B. *Phys. Rev. B* **1992**, *45*, 11372.
(27) Lanczos, C. *J. Res. Natl. Bur. Stand.* **1950**, *45*, 255.
(28) Johnson, D. D. *Phys. Rev. B* **1988**, *38*, 12807.
(29) Wood, D. M.; Zunger, A. *J. Phys. A* **1985**, *18*, 1343.
(30) Kresse, G.; Furthmüller, J. *Phys. Rev. B* **1996**, *54*, 11169.
(31) Teter, M. P.; Payne, M. C.; Allan, D. C. *Phys. Rev. B* **1989**, *40*, 12255.
(32) Payne, M. C.; Teter, M. P.; Allan, D. C.; Arias, T. A.; Joannopoulos, J. D. *Rev. Mod. Phys.* **1992**, *64*, 1045.
(33) Car, R.; Parrinello, M. *Phys. Rev. Lett.* **1985**, *55*, 2471.
(34) Tassone, F.; Mauri, F.; Car, R. *Phys. Rev. B* **1994**, *50*, 10561.
(35) Press, W. H.; Teukolsky, S. A.; Vetterling, W. T.; Flannery, B. P. *Numerical Recipes*; Cambridge University Press: New York, 1992.
(36) Ramer, N. J.; Rappe, A. M. *Phys. Rev. B* **1999**, *59*, 12471.
(37) Hamann, D. R.; Schlüter, M.; Chiang, C. *Phys. Rev. Lett.* **1979**, *43*, 1494.
(38) Kleinman, L.; Bylander, D. M. *Phys. Rev. Lett.* **1982**, *48*, 1425.
(39) Rappe, A. M.; Rabe, K. M.; Kaxiras, E.; Joannopoulos, J. D. *Phys. Rev. B* **1990**, *41*, 1227.
(40) Gonze, X.; Käckell, P.; Scheffler, M. *Phys. Rev. B* **1990**, *41*, 12264.
(41) Gonze, X.; Stumpf, R.; Scheffler, M. *Phys. Rev. B* **1991**, *44*, 8503.
(42) Koelling, D. D.; Harmon, B. N. *J. Phys. C* **1977**, *10*, 3107.
(43) Bachelet, G. B.; Schlüter, M. *Phys. Rev. B* **1982**, *25*, 2103.
(44) Walter, E. J.; Rappe, A. M. *Surf. Sci.* **1999**, *428*, 11.
(45) Becke, A. D. *J. Chem. Phys.* **1992**, *97*, 9173.
(46) Huber, K. P.; Herzberg, G. *Molecular spectra and molecular structure 4*; Van Nostrand Reinhold Company: New York, 1979.
(47) Taylor, S.; Lemire, G. W.; Hamrick, Y. M.; Fu, Z.; Morse, M. D. *J. Chem. Phys.* **1988**, *89*, 5517.
(48) Gupta, S. K.; Nappi, B. M.; Gingerich, K. A. *Inorg. Chem.* **1981**, *20*, 966.
(49) Miedema, A. R. *Faraday Symp. Chem. Soc.* **1980**, *14*, 136.
(50) Miedema, A. R.; Gingerich, K. A. *J. Phys. B* **1979**, *12*, 2081.
(51) Miedema, A. R.; Gingerich, K. A. *J. Phys. B* **1979**, *12*, 2255.
(52) Balasubramanian, K. *J. Chem. Phys.* **1987**, *87*, 6573.
(53) Zurita, S.; Rubio, J.; Illas, F.; Barthelat, J. C. *J. Chem. Phys.* **1996**, *104*, 8500.
(54) Harris, J. *Phys. Rev. B* **1985**, *31*, 1770.

(55) Yang, S. H.; Drabold, D. A.; Adams, J. B.; Ordejón, P.; Glassford, K. *J. Phys.: Condens. Matter* **1997**, *9*, L39.
(56) Kua, J.; Goddard, W. A., III. *J. Phys. Chem. B* **1998**, *102*, 9481.
(57) Jahn, H. A.; Teller, E. *Proc. R. Soc. London* **1937**, *A161*, 220.
(58) Dai, D.; Balasubramanian, K. *J. Chem. Phys.* **1995**, *103*, 648; **2000**, *113*, 7919; **2000**, *113*, 7928.
(59) Watari, N.; Ohnishi, S. *Phys. Rev. B* **1998**, *58*, 1665.
(60) Reddy, B. V.; Khanna, S. N.; Dunlap, B. I. *Phys. Rev. Lett.* **1993**, *70*, 3323.
(61) Menon, M.; Connolly, J.; Lathiotakis, N.; Andriotis, A. *Phys. Rev. B* **1994**, *50*, 8903.
(62) Goodwin, L.; Salahub, D. R. *Phys. Rev. A* **1993**, *47*, R774.
(63) Wesendrup, R.; Hunt, T.; Schwerdtfeger, P. *J. Chem. Phys.* **2000**, *112*, 9356.
(64) Arratia-Perez, R.; Ramos, A. F.; Malli, G. L. *Phys. Rev. B* **1989**, *39*, 3005.
(65) Rao, B. K.; Jena, P.; Manninen, M. *Phys. Rev. Lett.* **1984**, *53*, 2300.
(66) Hishinuma, N. *J. Chem. Phys.* **1996**, *105*, 5358.
(67) Kumar, V.; Bhattacharjee, S.; Kawazoe, Y. *Phys. Rev. B* **2000**, *61*, 8541.
(68) Yi, J.; Oh, D. J.; Bernholc, J. *Phys. Rev. Lett.* **1991**, *67*, 1594.
(69) Tománek, D.; Schlüter, M. A. *Phys. Rev. Lett.* **1986**, *56*, 1055.
(70) Moravec, V. D.; Klopcic, S. A.; Jarrold, C. C. *J. Chem. Phys.* **1999**, *110*, 5079.
(71) Kittel, C. *Introduction to Solid State Physics* 23, 55, and 530; John Wiley & sons: New York, 1986.
(72) Yeo, Y. Y.; Vattuone, L.; King, D. A. *J. Chem. Phys.* **1997**, *106*, 392.
(73) Brown, W. A.; Kose, R.; King, D. A. *Chem. Rev.* **1998**, *98*, 797.
(74) Parker, D. H.; Bartram, M. E.; Koel, B. E. *Surf. Sci.* **1989**, *217*, 489.
(75) Winkeler, A.; Guo, X.; Siddiqui, H. R.; Hagans, P. L.; Yates, J. T., Jr. *Surf. Sci.* **1988**, *201*, 419.
(76) Campbell, C. T.; Ertl, G.; Kuipers, H.; Segner, J. *Surf. Sci.* **1981**, *107*, 220.
(77) Gland, J. L.; Sexton, B. A.; Fisher, G. B. *Surf. Sci.* **1980**, *95*, 587.
(78) Astegger, S.; Bechtold, E. *Surf. Sci.* **1982**, *122*, 491.
(79) Starke, U.; Materer, N.; Barbieri, A.; Döll, R.; Heinz, K.; Van Hove, M. A.; Somorjai, G. A. *Surf. Sci.* **1993**, *287/288*, 432; **1995**, *325*, 207.
(80) Hayek, K.; Glassl, H.; Gutmann, A.; Leonhard, H.; Prutton, M.; Tear, S. P.; Welton-Cook, M. R. *Surf. Sci.* **1985**, *152/153*, 419.
(81) Jennison, D. R.; Schultz, P. A.; Sears, M. P. *Phys. Rev. Lett.* **1996**, *77*, 4828.